Materials Advances

ROYAL SOCIETY OF CHEMISTRY

PAPER

View Article Online
View Journal | View Issue

Cite this: *Mater. Adv.*, 2021, 2, 7445

A functionalization study of aerosol jet printed organic electrochemical transistors (OECTs) for glucose detection†

Jiaxin Fan, Andres Alejandro Forero Pico and Manisha Gupta *

In this work, we have conducted a functionalization study of organic electrochemical transistors (OECTs) for glucose detection. The functionalization method of a biosensing device strongly affects its sensitivity and range of detection. Here, a glucose sensing study was performed on aerosol jet (AJ) printed OECTs *via* four different functionalization configurations: unfunctionalized device with floating GOx, PEDOT:PSS channel functionalized with GOx, printed Pt gate functionalized with GOx, and sputtered Pt gate functionalized with GOx, in order to study the effect of the functionalization site and the utilized nanomaterials on the sensing range and sensitivity. We found that the printed OECT with the GOx functionalized printed Pt gate exhibits the best performance. It demonstrates a large glucose (in PBS solution) detection range between 100 nM and 50 mM with two sensitivities of 0.022 NR per dec for 100 nM to 250 μM and 0.255 NR per dec for 250 μM to 50 mM. The OECT with the functionalized printed Pt gate was then evaluated for the detection of glucose in an artificial sweat buffer, demonstrating a detection range of 0.1 to 10 mM with two linear slopes of 0.068 NR per dec for 100 nM–500 μM and 0.384 NR per dec for 500 μM–10 mM. Also, AJ printing and laser sintering offer the benefit of simultaneous deposition and patterning of materials and rapid annealing of materials, and hence, they simplify the fabrication process and reduce the fabrication cost. These results confirm that these functionalized printed OECT based sensors are highly promising for application as non-invasive electrochemical glucose sensors. Thus, clearly for biosensor development, the choice of the functionalization site and material is very important.

Received 31st May 2021,
Accepted 12th September 2021

DOI: 10.1039/d1ma00479d

rsc.li/materials-advances

1. Introduction

Fast and precise portable glucose detection is an increasingly important requirement as the diabetic population is increasing and is expected to reach ~700 million by 2045.[1] Glucose concentration in blood has been widely used as a disease biomarker for the diagnosis of diabetes. As indicated by the American Diabetes Association (ADA), diabetes not only is a concern for individuals, but also poses a significant burden to the healthcare system with the average annual cost of diagnosed diabetes increasing by 26% from 2012 to 2017 considering inflation.[2] Monitoring the episodes of hyperglycemia and severe hypoglycemia in diabetic patients is important to manage their conditions. Therefore, biosensors for measuring the glucose level have been rapidly developed, which also drives the market growth for glucose biosensors. In 2015, the market value of glucose biosensors was estimated at 15.3 billion USD, in which the homecare diagnostic segment, such as point-of-care glucose meters, accounts for the largest share of 46%.[3] The most used self-testing glucose meters are finger-pricking devices. They are based on different types of enzyme modified electrochemical electrodes. A blood sample needs to be collected from the patient's fingertip for each measurement. Therefore, in finger-pricking devices, the reading reflects the blood glucose level for the time window of the blood sampling, and the blood sampling process could be inconvenient for taking the measurements frequently.

A continuous glucose monitor (CGM) is a wearable device that measures the skin interstitial fluid glucose level at regular intervals and 24/7. A CGM provides more information about the glycemic variability of an individual and alters the current as well as the impending hyper- and hypoglycemia. It can also be used in conjunction with an insulin pump to reduce the risk of hypoglycemia in patients.[4] Despite its potential benefits for glycemic control, the clinical implementation of a CGM is still limited due to its disadvantages such as regular calibration requirement with a blood glucose meter, sensor accuracy and reliability, and high cost.[4,5]

Department of Electrical and Computer Engineering, University of Alberta, Edmonton, Alberta, T6G 1H9, Canada. E-mail: mgupta1@ualberta.ca

† Electronic supplementary information (ESI) available. See DOI: 10.1039/d1ma00479d

Studies have shown that salivary[6] and sweat[7] glucose levels reflect the changes in the blood glucose level and therefore can be used as a monitoring tool to assess the glycemic status of diabetic patients. These studies have offered an opportunity for the development of affordable, non-invasive, and highly sensitive disposable glucose sensors to aid diabetes management. Organic electrochemical transistors (OECTs) have been extensively used as biological and chemical sensors for detecting pH,[8] ions,[9–11] lactate,[12–14] dopamine,[11,15,16] uric acid,[17] DNA,[18] cells[19] and proteins.[20] Organic electrochemical transistors (OECTs) represent a type of organic thin film transistors (OTFTs), and they exhibit several advantages for biosensing applications, such as intrinsic signal amplification, low operating voltages, and the ability to operate in an aqueous environment. An OECT consists of a metal source and drain contact, a conducting polymer channel, an aqueous or gel electrolyte in direct contact with the channel, and a metal gate electrode immersed in the electrolyte. The operation of an OECT relies on the electrochemical doping/dedoping of the active channel material due to the injection of ions from the electrolyte driven by the gate bias.

To develop a high-performance biosensor, functionalization of the transducer surface is a critical step in improving the sensitivity and more importantly in achieving selectivity to the analyte of interest. Various functionalization configurations have been implemented with OECTs to expand their applications in biosensing.[21] Two commonly used categories of immobilization techniques are physisorption and chemisorption. Physisorption is the simplest method for macromolecule immobilization. In this case, the surface functionalization is achieved by immersing the surface in the biomolecule solution for fixed durations, and the biomolecules are bound to the surface *via* weak forces, such as van der Waals and electrostatic forces. Physisorption is a cost-effective method, and the conformation and activity of the biomolecules are well preserved after immobilization.[22] Some limitations of physisorption are desorption from the carrier surface and low immobilization efficiency.[23] Chemisorption normally requires multiple steps, in which the surface is first modified with functional groups and then the biomolecules are attached to the surface *via* strong covalent bonds. Chemisorption forms strong linkages between the biomolecules and the surface, and hence the modified surface becomes more stable. With the assistance of self-assembled monolayers (SAM), site-directed attachment can be achieved, which results in a more homogenous surface and improves the immobilization efficiency.[22] However, chemisorption may involve toxic solvents and chemicals, and the biomolecules may lose their functional conformation after immobilization.[23] Nanomaterials have unique properties and are applied in various fields. For the development of biosensor devices, nanomaterials have been demonstrated to enhance the immobilization of biomolecules and promote the desired electrochemical reaction due to their large surface area.[23,24]

Another key factor to consider in biosensor design is the region of modification. For an OECT, the channel and gate are the two main sites for functionalization as they are in direct contact with the electrolyte and the analyte. Depending on the requirements for specific analyte detection and sensing mechanism, each functionalization site has its advantages. When the channel is functionalized, the interaction between the analyte and the channel leads to a direct device response.[25] The modification of the channel interface leads to a change in the interfacial potential, and the binding of the analyte modulates the channel current.[26–28] However, certain functionalization techniques damage the channel material, which results in poor sensing performance. Meanwhile, for gate functionalization, the channel remains intact after modification. Furthermore, as OECTs have a high transconductance (g_m), any small changes at the gate caused by the interaction with the analyte will be transduced into apparent changes in the channel current.[25] OECTs are commonly fabricated using microfabrication techniques, but they can also be fabricated by various printing techniques such as screen printing,[29] inkjet printing, 3D printing[9,30,31] and aerosol jet (AJ) printing.[32,33] Printing technologies provide the benefits of versatility and wide-range material compatibility, and they allow patterning and deposition of the material for each layer simultaneously, which reduces the number of steps and the cost of fabrication.[25] As compared to other printing techniques, AJ printing is a non-contact technique, and by utilizing a sheath gas flow along with the carrier gas flow it is possible to print features with sizes that are a fraction of the nozzle size.

In the past two decades, quite a few research groups have demonstrated OECT based glucose sensors, both functionalized and unfunctionalized, which exhibited low limits of detection, high sensitivity, and high linearity ranges.[34–37] Here, we have conducted a detailed study of which OECT functionalization configuration works the best for glucose sensing. We used fully aerosol jet printed OECTs with a Ag source and drain contact, a poly(3,4-ethylenedioxythiophene):polystyrene sulfonate (PEDOT:PSS) channel, and a printed/sputtered in-plane Pt gate. The detection of glucose was carried out using the printed OECT with glucose oxidase (GOx) in four different configurations: unfunctionalized OECT with floating GOx, functionalized channel, functionalized printed Pt gate, and functionalized sputtered Pt gate. The physisorption technique was utilized for GOx immobilization for all the functionalization cases in this work. The performances of these four types of sensors were evaluated in terms of their detection range, sensitivity, and feasibility as sweat glucose sensors. The sensor speed was not evaluated in this work as the response time of the OECT depends mainly on its channel thickness and ionic transportation,[38,39] which were kept the same for all four functionalization configurations. From this study, we observed that the functionalized printed Pt gate demonstrated the best glucose sensing performance. This is due to the higher surface area of the printed nanoparticle-based Pt gate, which makes it very effective for GOx adsorption.

2. Materials and methods

2.1. Device fabrication

OECTs were printed on polyimide films (Kapton type HN films purchased from Cole-Parmer, 25.4 μm thick) using an Optomec

Aerosol Jet 5-axis (AJ5X) 3D printing system, which was equipped with two atomizers: ultrasonic (UA) and pneumatic (PA). The UA and PA were used to dispense low and high viscosity materials, respectively. The device layouts were designed using AutoCAD 2018 software and exported as a compatible script for printing by VMTools developed by Optomec. A commercially available silver (Ag) nanoparticle (NP) ink (Clariant EXPT Prelect TPS 50G2) was first diluted with deionized (DI) water at a volume (v/v) ratio of 1 : 1. The diluted Ag NP ink was then used for printing the source and drain contacts of OECTs using the UA. Two layers of wet printing were used to ensure the continuity of the resulting Ag traces. The thickness of the Ag film was 2.44 ± 0.03 μm after curing in an oven overnight at 130 °C and the average conductivity was 2×10^5 S cm^{-1}. A conductive platinum (Pt) nanoparticle (NP) ink (UT DOTS, INC.) was used for printing the in-plane gate electrode for OECTs. The Pt NP patterns were laser-sintered using an 830 nm laser with a 100 mW power. The resulting Pt film had an average thickness of 200 ± 4 nm and a conductivity of 7.05 S cm^{-1}. The PEDOT:PSS ink was prepared by mixing PEDOT:PSS (Clevios PH-1000) solution with 20% ethylene glycol (EG) (Sigma-Aldrich), 0.1% dodecylbenzenesulfonic acid (DBSA) (Sigma-Aldrich), and 0.9% (3-glycidyloxypropyl)trimethoxysilane (GOPS) (Sigma-Aldrich), then sonicated for 1 hour and filtered through a 0.45 μm nylon syringe filter to remove any large particles. The filtered ink was then deposited using the UA to form the channel region on the printed Ag source and drain. UV-curable polydimethylsiloxane (PDMS) (Shin-Etsu KER-4690A/B) solution was used to passivate the source and drain electrodes to prevent shorting from the electrolyte. The PDMS solution was diluted with hexane at a v/v ratio of 3 : 1. The diluted PDMS ink was dispensed on the electrodes using the PA and cured on-the-fly with UV (405 nm and 5 mW). A final bake at 130 °C for 30 min was performed on a hotplate to ensure that the PDMS layer was fully crosslinked.

For devices with the sputtered Pt gate electrode, a silicon (Si) wafer coated with a 500 nm thermal oxide (SiO_2) layer was used as the substrate. The SiO_2/Si wafer was cleaned in piranha solution for 15 min, thoroughly rinsed with DI water and dried with nitrogen. The wafer was immediately treated in an automatic hexamethyldisilizane (HMDS) vapour prime oven to promote photoresist adhesion. After patterning with the AZ5214 photoresist and MF390 developer, a 10 nm layer of titanium (Ti) and a 100 nm layer of platinum (Pt) were subsequently deposited using a magnetron sputtering system, and lift-off was performed in acetone to form the Pt gate electrode. The OECT devices were then printed on the SiO_2/Si substrate and next to the patterned Pt gate electrode using the same steps mentioned above.

2.2. Enzyme immobilization

Glucose oxidase (GOx) (from *Aspergillus niger*, Sigma-Aldrich, G2133) was first dissolved in 1× phosphate buffer saline (PBS) (Fisher Scientific) solution (pH = 7.4) to prepare 32 mg mL^{-1} GOx solution. 1 wt% CHIT solution was prepared by dissolving low molecular weight chitosan (CHIT) (Sigma-Aldrich) in 1% acetic acid (Sigma-Aldrich). The GOx and CHIT solutions were mixed with a volume ratio of 1 : 1 to prepare the final stock solution for functionalization with a GOx concentration of 16 mg mL^{-1}. To functionalize the OECT, 3 μL of the GOx stock solution was drop-casted using a micropipette onto the channel or the gate region. The device was left to dry for 72 hours at 4 °C. After the GOx immobilization, the functionalized area of the device was rinsed three times with PBS solution and finally with DI water to remove any loose material. The devices were then tested. The enzyme stock solution concentration was optimized based on the performance of OECT based glucose sensors with the functionalized channel and printed Pt gate. Fig. S1 (ESI†) shows the real time I_D measured for OECTs functionalized with 3 μL of 8 mg mL^{-1} GOx stock solution. Smaller detection ranges of 0.2 to 2 mM and 0.1 to 5 mM were observed for OECTs with the functionalized channel and functionalized printed gate, respectively. These ranges are not sufficient for detecting the glucose level in sweat. Therefore, the final GOx stock solution of 16 mg mL^{-1} was used to extend the range of detection.

2.3. Device characterization

All the electrical measurements were performed at room temperature using a Keithley 2612B source meter controlled by LabVIEW. Each device was characterized using 1× PBS solution as the electrolyte and the printed in-plane Pt gate to evaluate the device performance before functionalization. The current–voltage (*I–V*) characteristics of the devices were measured by biasing the gate voltage (V_G) from 0 V to 1 V with a step size of 0.1 V while sweeping the drain voltage (V_D) from 0.2 V to −0.8 V with a step size of −0.02 V and measuring the drain current (I_D). The transfer curve (I_D *vs.* V_G) and transconductance ($g_m = \Delta I_D/\Delta V_G$) were extracted from the *I–V* characteristics of the devices.

Glucose sensing was conducted by biasing the OECT with a constant V_D value (−0.2 V) and a constant V_G value (0.6 V) and measuring the I_D value as a function of time. Initially, 5 μL of PBS solution was added as the background electrolyte, and then 5 μL of D-glucose (Sigma-Aldrich) dissolved in PBS with increasing concentrations (100 nM to 50 mM) was consecutively added to the electrolyte at fixed time intervals. For floating GOx experiments, 3 μL of GOx solution (16 mg mL^{-1} in PBS) was added to the electrolyte before adding glucose solutions.

To compare the glucose sensitivity over different devices, the change of drain current after adding different concentrated glucose solutions was normalized as follows:

$$\mathrm{NR} = \left| \frac{I_D^{\mathrm{conc}=0} - I_D^{\mathrm{conc}>0}}{I_D^{\mathrm{conc}=0}} \right| \quad (1)$$

where NR is the normalized I_D response; $I_D^{\mathrm{conc}=0}$ represents the drain current before adding glucose to the electrolyte; and $I_D^{\mathrm{conc}>0}$ is the drain current after adding glucose solution of a specific concentration.

An artificial sweat buffer containing 20 g L^{-1} NaCl, 17.5 g L^{-1} NH_4Cl, 5 g L^{-1} acetic acid and 15 g L^{-1} lactic acid was prepared according to the ISO standard ISO-3160-2, and the pH of the solution was adjusted to 4.7 using sodium hydroxide (NaOH). Glucose sensing was conducted in the artificial sweat buffer using the same procedure as the one used for glucose sensing in PBS.

3. Results and discussion

3.1. Sensor design and sensing mechanism

Fig. 1 shows the microscopic images of the OECT based glucose sensors developed in this work using four functionalization configurations. For the unfunctionalized OECT with floating GOx, the OECT with the printed Pt gate was directly used for glucose detection with GOx being added to the electrolyte during the measurement. In this case, there was no loss in the enzyme amount, and the biofunction of the enzyme remained unaffected. For the functionalized channel, GOx was immobilized onto the channel of the OECT *via* physisorption as shown in Fig. 1(b). This configuration was compared with the OECT with the functionalized printed Pt gate to determine which functionalization site is preferable. To study the effect of nanomaterials, two functionalized gate configurations were utilized: Pt gate deposited by magnetron sputtering and printed Pt gate using nanoparticle-based ink. All the OECTs used in this work have similar dimensions: a gate size of 1 mm^2, a channel length of 100 μm with an average channel width-to-length ratio of 4 and an average channel thickness of 560 nm.

Fig. 2(a) and (b) show the typical output and transfer characteristics of a printed unfunctionalized OECT measured with the printed Pt gate and PBS solution as the electrolyte. When both the channel and the gate electrode are immersed in an electrolyte and a positive gate bias is applied, the cations in the electrolyte penetrate the channel and compensate the negative charges on PSS, reducing PEDOT to its less conducting neutral state. This leads to a decrease in the magnitude of drain current. From the transfer characteristics (Fig. 2(b)), we observed that these printed OECTs exhibit a typical p-type depletion (normally ON) mode behavior as expected. An overall gate to drain bias difference of less than 1 V is preferred in order to avoid water electrolysis. Hence, a constant drain bias, V_D, of −0.2 V was selected for the glucose spike tests. From the transconductance (g_m) curves (Fig. 2(c)), the maximum transconductance ($g_{m,max}$) for $V_D = -0.2$ V appears near a V_G value of 0.6 to 0.7 V. Therefore, to maximize the device sensitivity, a gate bias, V_G, of 0.6 V was used for conducting the real time glucose sensing, I_D, measurements.

The glucose sensing mechanism using GOx for functionalization has been explained by other research groups.[35,40–42] This is based on the enzymatic reaction of GOx and the glucose molecules and the oxidation of hydrogen peroxide (H_2O_2) at the Pt gate electrode under positive bias as shown in the following chemical reactions:

$$\text{D-glucose} + O_2 \xrightarrow{\text{GOx}} \text{D-glucono-1, 5-lactone} + H_2O_2 \quad (2a)$$

$$H_2O_2 \rightarrow O_2 + 2H^+ + 2e^- \quad (2b)$$

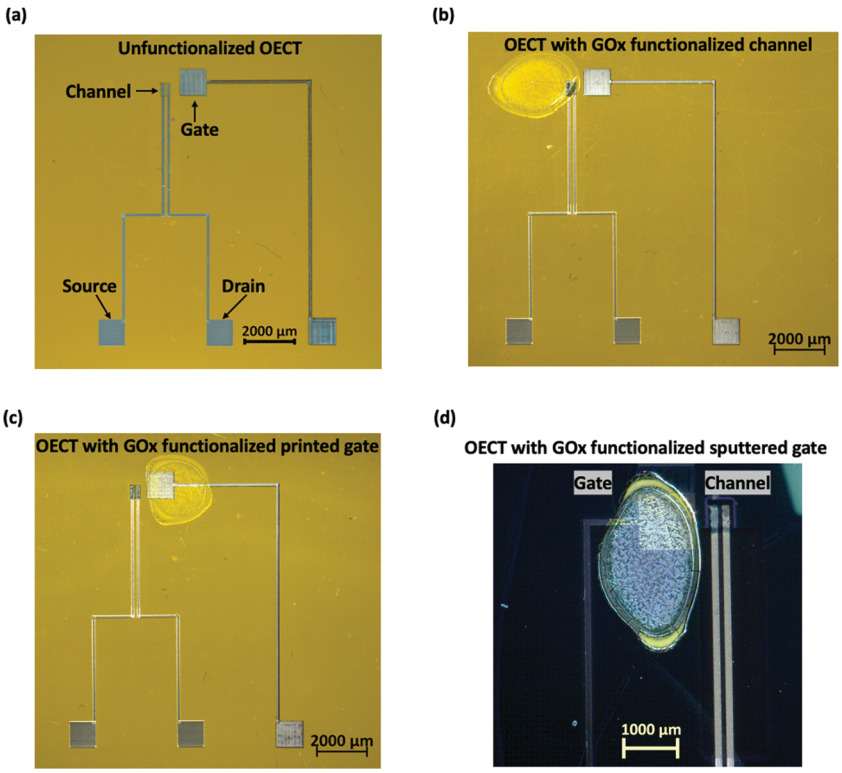

Fig. 1 Printed OECT based glucose sensors developed in this work. (a) Microscopic image of a printed unfunctionalized OECT on a Kapton substrate with a printed Ag source and drain contact, a PEDOT:PSS channel, and an in-plane Pt gate without any modifications. The metal traces were passivated with a PDMS mask to prevent shorting during the measurement. (b) Microscopic image of a fully printed OECT on a Kapton substrate with a channel functionalized with GOx for glucose sensing. (c) Microscopic image of a printed OECT on a Kapton substrate with a GOx functionalized printed Pt gate for glucose sensing. (d) Microscopic image of a printed OECT on a SiO_2/Si substrate with a GOx functionalized sputtered Pt gate.

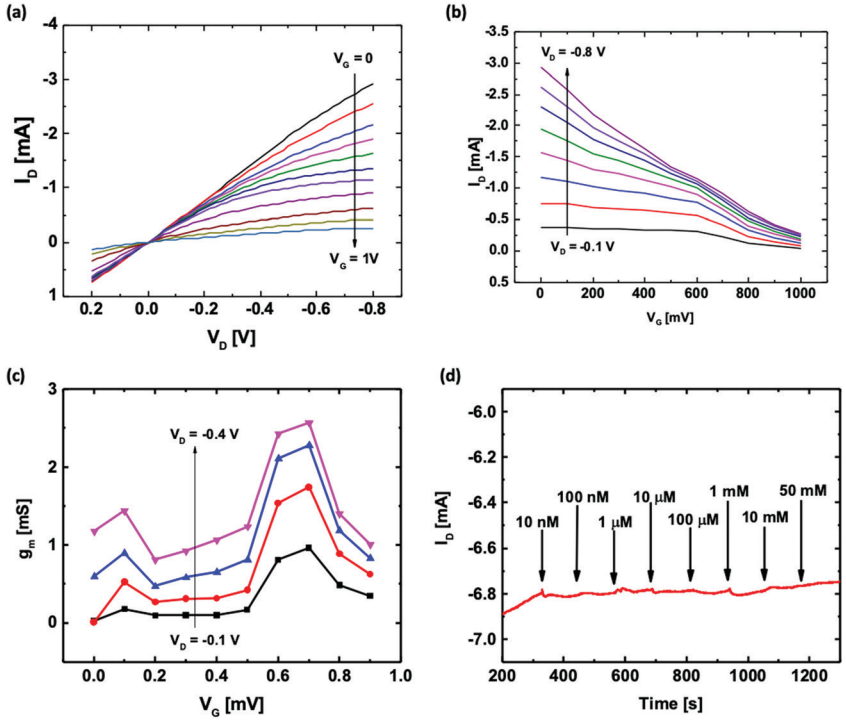

Fig. 2 (a) Typical output characteristics of a printed OECT measured with PBS electrolyte at different V_G values (0 to 1 V). (b) Transfer characteristics at different V_D values (−0.1 V to −0.8 V) of a printed unfunctionalized OECT. (c) g_m curves extracted for V_D values ranging from −0.1 to −0.4 V. (d) I_D shows a negligible change with the increase in glucose concentration for an OECT without any GOx functionalization.

where O_2 is the oxygen molecule, H^+ is the hydrogen ion, and e^- represents the electron. As small enough voltages are selected to bias the OECT to prevent the electrolysis of water, the device operates in the non-faradaic regime. From the reaction shown in eqn (2a), it can be observed that the D-glucose molecules are oxidized to D-glucono-1,5-lactone under the catalytic effect of GOx. The H_2O_2 produced in the process is proportional to the initial glucose concentration. As shown in the reaction in eqn (2b), the dissociation of H_2O_2 molecules is catalyzed by Pt and this induces electron transfer (faradaic current) to the Pt gate electrode. This faradaic contribution can be described by Nernst's equation. Since the device is under constant bias, the faradaic current due to H_2O_2 decomposition changes the potential distribution across the gate electrolyte and channel interface, which leads to an increase in the effective gate voltage (V_G^{eff}) and a decrease in the magnitude of the drain current ($|I_D|$).[34] Therefore, a decrease in $|I_D|$ is expected as the electrolyte glucose concentration increases, which can be used for glucose detection.

3.2. Sensor performance comparison

To evaluate and compare the performance of the four types of OECT based glucose sensors, the OECTs were biased under constant drain and gate voltages (V_G = 0.6 V and V_D = −0.2 V). The I_D was then measured as a function of time with the addition of increasing concentrations of the glucose solution directly into the electrolyte. Fig. 2(d) shows that the unfunctionalized OECT, without GOx in the electrolyte, exhibits a negligible I_D change with an increase in glucose concentration up to 50 mM. Thus, the unfunctionalized OECT cannot be directly used for the detection of glucose concentration.

Fig. 3 shows the I_D responses of the OECTs with four different functionalization configurations to the addition of glucose solution. Fig. 3(a) shows the real-time I_D response of the floating GOx case, in which an unfunctionalized OECT with 3 μL of GOx solution was added to the electrolyte before adding glucose and measured with a printed Pt gate. Fig. 3(b) shows the I_D response of a printed OECT with GOx being physically adsorbed onto the PEDOT:PSS channel region and measured using a printed Pt gate. Fig. 3(c) and (d) show the I_D responses of an OECT with the GOx functionalized printed Pt gate and an OECT with the GOx functionalized sputtered Pt gate, respectively. For all four different cases, a clear shift of I_D was observed after each glucose addition. As expected, the magnitude of I_D decreases as the glucose concentration increases. The corresponding gate current (I_G) responses of the OECTs during the glucose measurement for the four functionalization configurations offer additional evidence of the generation of faradaic current as shown in Fig. S2 (ESI†). For the first few glucose concentrations, the current response is much lower compared to the higher glucose concentration measurements because there is a lower number of glucose molecules. The real-time I_D response in Fig. 3 was used to extract the normalized drain current response for the four different functionalization configurations to compare the device sensitivities. The normalized I_D response (NR) was then plotted against the logarithmic

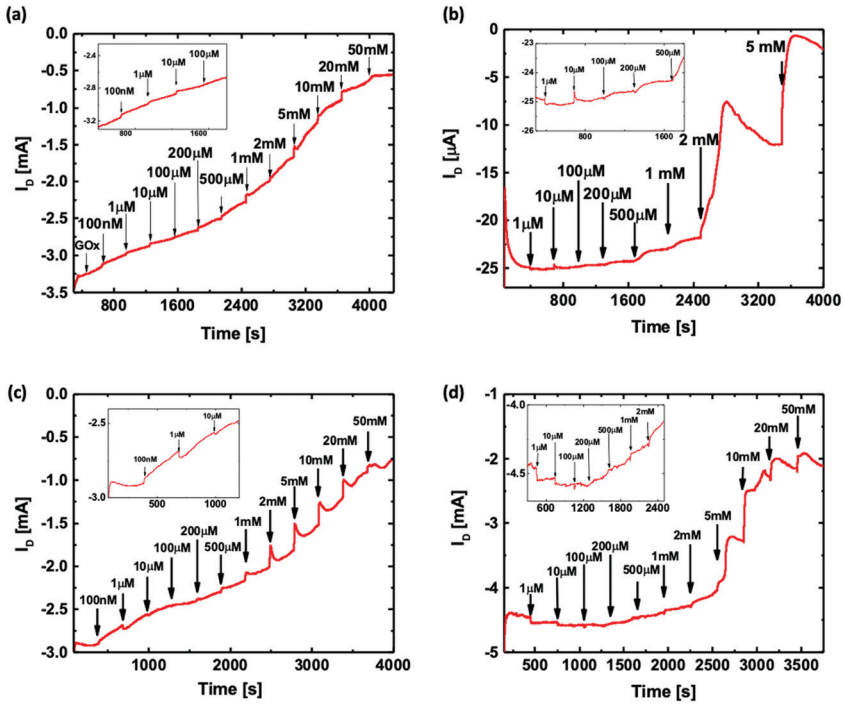

Fig. 3 I_D response of printed OECTs to the addition of glucose solution under constant biases (V_G = 0.6 V and V_D = −0.2 V). (a) I_D response of an unfunctionalized OECT measured with a printed Pt gate and floating GOx (inset: I_D response to the addition of glucose at concentrations ranging from 100 nM to 100 μM). (b) I_D response of an OECT with the channel functionalized with GOx and a printed Pt gate (inset: I_D response to the addition of glucose at concentrations ranging from 1 μM to 500 μM). (c) I_D response of an OECT with a GOx functionalized printed Pt gate (inset: I_D response to the addition of glucose at concentrations ranging from 100 nM to 10 μM). (d) I_D response of a printed OECT with a functionalized sputtered Pt gate (inset: I_D response to the addition of glucose at concentrations ranging from 1 μM to 2 mM).

glucose concentration as shown in Fig. 4. Fig. 4(a) shows the NR of the floating GOx case averaged over three different devices. In this case, two distinctive linear regions were observed; a correlation coefficient (R) of 0.993 and a sensitivity of 0.020 NR per dec were obtained for the glucose concentration range of 100 nM–153 μM, and R = 0.991 and a higher sensitivity of 0.283 NR per dec were obtained for the range of 153 μM–50 mM. Fig. 4(b) demonstrates the NR of OECTs with the functionalized channel averaged over three different devices. I_D scaled linearly with a slope of 0.019 NR per dec for the range of 1–413 μM and a second linear slope of 0.254 NR per dec for the range of 413 μM–2 mM was observed in this case. Fig. 4(c) shows the average NR of three different OECTs with the functionalized printed Pt gate, and two sensitivity regions were also observed here with 0.022 NR per dec and R = 0.983 for the lower glucose concentration range of 100 nM–250 μM, and 0.255 NR per dec and R = 0.976 for the higher glucose concentration range of 250 μM–50 mM. Fig. 4(d) shows the average NR of three OECTs with the functionalized sputtered Pt gate. There are also two sensitivity regions in this case. A sensitivity of 0.015 NR per dec and R = 0.965 were obtained for the range of 1 μM–1 mM, and a sensitivity of 0.314 NR per dec and R = 0.960 were obtained for the glucose concentration range of 1–50 mM. Two linear slopes were observed for each OECT functionalization configuration. Since a fixed number of GOx molecules were presented in each functionalization configuration, for the initial low glucose concentration sensing, there were enough free GOx molecules to convert all the added glucose molecules. Thus, as the glucose concentration kept increasing, all the GOx molecules had reacted which led to a reduction in the reaction rate. In addition, as the glucose concentration increased, the produced H_2O_2 molecules also increased. Since the Pt surface area was fixed for each functionalization configuration, the dissociation of H_2O_2 molecules was limited by the surface area at higher glucose concentrations instead of the H_2O_2 molecule diffusion rate for lower glucose concentrations. The changes in the reaction rate may be the reason why we observe the two sensitivity ranges for these OECT based glucose sensors.

Fig. 4(e) shows the average NR extracted for all the four functionalization configurations plotted in the same graph. For the unfunctionalized OECT with floating GOx, since the device was unfunctionalized and the GOx solution was directly added to the electrolyte, the device performance and the quantity and activity of the enzymes were fully preserved. Hence, the OECT responded to a large range of glucose concentrations (100 nM to 50 mM). However, this configuration is not suitable for the development of non-invasive glucose sensors as it requires an additional step of adding the enzyme prior to the test, which could induce potential issues such as inconvenience in testing, additional requirements for the storage and transportation of the enzyme solution, and calibration and/or measurement

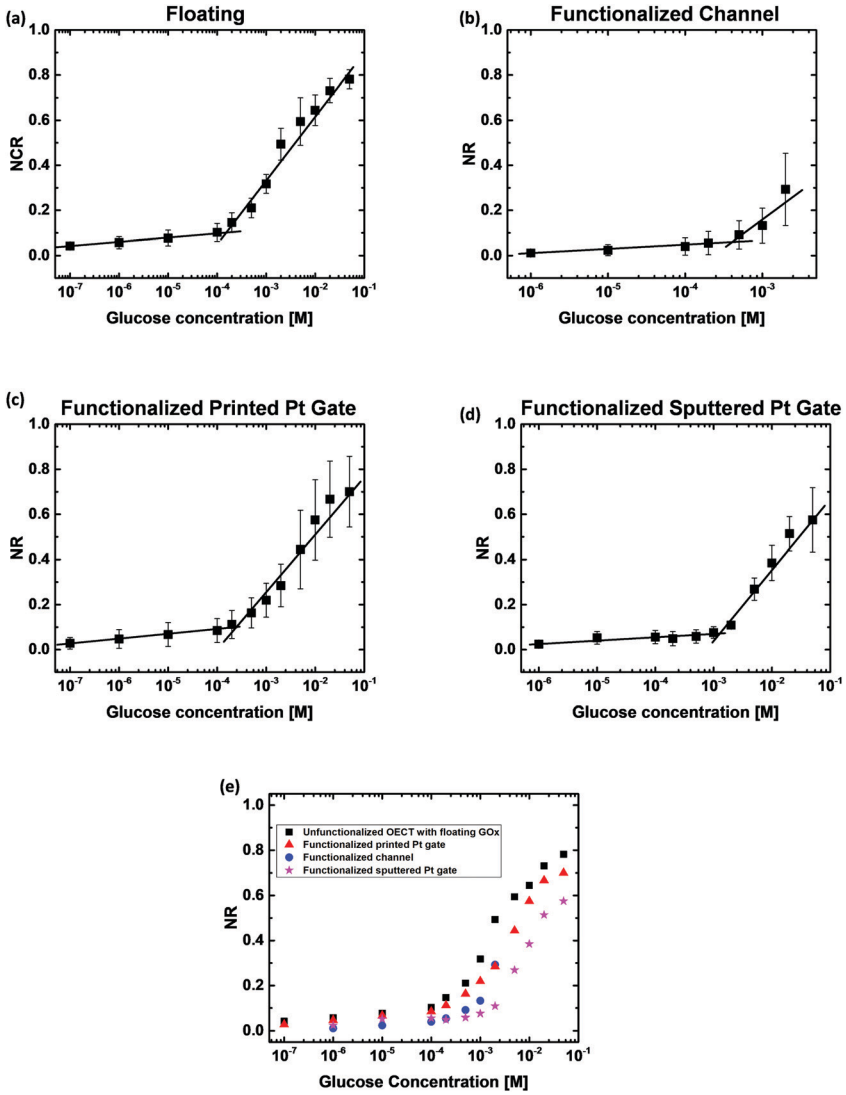

Fig. 4 Normalized I_D responses (NR) of OECTs to the logarithmic glucose concentration. (a) The average NRs of OECTs with floating GOx and a printed Pt gate showing two linear regions with a slope of 0.020 NR per dec for the glucose concentration range of 100 nM to 153 μM and a slope of 0.283 NR per dec for the glucose concentration range of 153 μM to 50 mM. (b) The average NR of OECTs with a functionalized channel and a printed Pt gate with two linear regions showing a slope of 0.019 NR per dec for the glucose concentration range of 10 μM to 413 μM and a slope of 0.254 NR per dec for the glucose concentration range of 413 μM to 2 mM. (c) The average NR of OECTs with a functionalized printed Pt gate showing two linear regions with a slope of 0.022 NR per dec for the glucose concentration range of 100 nM to 250 μM and a slope of 0.255 NR per dec for the glucose concentration range of 250 μM to 50 mM. (d) The average NR of OECTs with a functionalized sputtered Pt gate showing two linear regions with a slope of 0.015 NR per dec for the glucose concentration range of 1 μM to 1.3 mM and a slope of 0.314 NR per dec for the glucose concentration range of 1.3 mM to 50 mM. (e) The average NR for all four functionalization methods plotted in the same graph. The error bars represent the standard error for all the plots.

errors due to the inconsistent enzyme amount. The printed OECTs with the functionalized channel demonstrated poor sensing performance, including a lower detection range of 10 μM to 5 mM and a lower I_D magnitude when compared to the other functionalization configurations. This is likely due to the degradation of the PEDOT:PSS film conductivity after GOx adsorption, which leads to a decrease in the device transconductance and hence a lower sensitivity. In addition, it took longer for the H_2O_2 molecules produced at the channel to diffuse to the Pt gate surface and become oxidized, which also contributed to the poor sensor performance. Therefore, the channel is not a favorable functionalization site for immobilizing GOx by the physisorption technique. The OECT with the functionalized printed Pt gate exhibited similar sensitivity and detection range to the unfunctionalized OECT with floating GOx, indicating that both the device sensitivity and enzyme bioactivity were not affected by the functionalization. This also indicated that the amount of GOx immobilized onto the gate surface is adequate for glucose detection in the desired concentration range. Additionally, since GOx is immobilized on the gate, it is more convenient to be directly used as a non-invasive glucose sensor. When compared with the channel functionalization, the gate is a more appropriate functionalization site to maintain the device performance. Even though the

printed OECT with the functionalized sputtered Pt gate exhibited the highest average sensitivity for a higher glucose concentration range (1.3 mM to 50 mM) among the four types of sensors, this sensor was found to be less sensitive for a lower glucose concentration range (1 μM to 1.3 mM), which is a more important range for developing sweat glucose sensors, as the glucose levels in sweat (0.277–1.11 mM)[7,43] are lower than those in blood (3–20 mM).[44] A higher surface roughness of the printed Pt nanoparticle-based film was observed in the scanning electron microscopy (SEM) and atomic force microscopy (AFM) images, as shown in Fig. S1 (ESI†). The RMS roughness (Rq) of the printed Pt thin film was 13.8 nm, which is approximately 16 times the value for the sputtered Pt thin film (Rq = 0.852 nm). The higher surface area of the printed Pt films facilitates more GOx adsorption per unit area and the electrochemical oxidation of H_2O_2, which results in a higher sensitivity for a lower glucose concentration range. Hence, among the four types of OECT based glucose sensors, we found that the printed Pt gate functionalization was the most suitable one for sweat glucose detection.

Our results along with those for some other OECT based glucose sensors reported in the literature are listed in Table 1. Several studies have utilized nanomaterials, such as nanoparticles and graphene, and demonstrated improvements in the limit of detection and sensor sensitivity due to their excellent electrical and chemical properties and, more importantly, higher surface area-to-volume ratios, which could improve the electrocatalysis and enzyme immobilization.[17,34,45] In our case, we have utilized a nanoparticle-based ink for printing the gate electrode and demonstrated an improvement in the limit of detection and sensitivity for lower concentration range as compared with the sample prepared using magnetron sputtering. In addition, utilizing the AJ printing technique we can achieve high particle density films by one-step nanoparticle ink patterning and deposition and rapid film annealing by laser sintering. Another key material used by many groups is biopolymers, such as CHIT and Nafion, which can improve enzyme immobilization due to their excellent biocompatibility.[17,34,45] Similarly, in this study, the OECT with the enzyme modified printed gate shows a similar detection range and sensitivity to the unfunctionalized OECT tested with floating GOx, indicating that the bioactivity of the enzyme is well preserved after immobilization.

3.3. Glucose sensing in the artificial sweat buffer

Glucose sensing in the artificial sweat buffer was conducted using the OECT with the functionalized printed Pt gate as it exhibited the best performance among the four functionalization configurations. The measurements were carried out by biasing the OECT at constant voltages (V_G = 0.6 V and V_D = −0.2 V) and using the artificial sweat buffer as the background electrolyte. Once I_D settled, 10 μL of glucose solutions dissolved in the artificial sweat buffer with concentrations of 100 μM, 500 μM, 1 mM, and 10 mM were consecutively added to the electrolyte, and the changes in I_D and I_G were recorded as shown in Fig. 5(a). A distinctive decrease in I_D (black curve) after each glucose addition could be observed, and the increase in I_G (blue curve) is a clear indication of the faradaic current due to H_2O_2 oxidation. This detection range covers the glucose levels found in human sweat (0.227–1.11 mM). When compared to the measurements conducted using PBS solution, I_D took a longer time to settle after each glucose solution addition. The slower response might be attributed to the composition and pH difference of the two types of buffer solutions, which leads to a slower molecule diffusion rate and a change in the enzymatic activity of GOx. Fig. 5(b) shows the corresponding normalized I_D response of the printed OECTs with the printed Pt gate averaged over three different devices. Similar to the measurements conducted in PBS solution, there are two sensitivity regions with a slope of 0.068 NR per dec and R = 1 for the sweat glucose concentration range of 100–500 μM and a slope of 0.384 NR per dec and R = 1 for the sweat glucose concentration range of 500 μM–10 mM.

Table 2 summarizes some previously reported transistor and electrode based sweat glucose biosensors along with our printed OECT based sweat glucose sensor. Most of these sweat glucose biosensors have utilized nanostructures or nanomaterials to increase the surface-to-volume ratio of the active area of the device for improving the sensing performance for low concentration detection. It has also been demonstrated that

Table 1 Comparison of the detection ranges and sensitivities of different types of OECT based glucose sensors

Channel material	Gate material	Sensing technique	Detection range	Sensitivity	Ref.
PEDOT:PSS	AJ printed Pt	Floating GOx	100 nM–153 μM 153 μM–50 mM	0.020 NR per dec 0.283 NR per dec	This work
CHIT/GOx/PEDOT:PSS	AJ printed Pt	Immobilized GOx	10–413 μM 413 μM–5 mM	0.019 NR per dec 0.254 NR per dec	This work
PEDOT:PSS	CHIT/GOx/AJ printed Pt	Immobilized GOx	100 nM–250 μM 250 μM–50 mM	0.022 NR per dec 0.255 NR per dec	This work
PEDOT:PSS	CHIT/GOx/Pt	Immobilized GOx	1 μM–1.3 mM 1.3–50 mM	0.015 NR per dec 0.317 NR per dec	This work
PEDOT:PSS	Pt	Floating GOx	1 μM–10 mM	0.01 NR per μM	46
PEDOT:PSS	Nafion/GOx/Pt NPs/TNTA	Immobilized GOx	100 nM–5 mM	0.0082 NR per dec	34
PPy/rGO	PPy/rGO/PA6/GOx/Nafion	Immobilized GOx	1 nM–5 μM	0.773 NR per dec	17
PEDOT:PSS	CHIT/GOx/Pt NPs/PEDOT:PSS/Au	Immobilized GOx	10 μM–5 mM	0.4762 NR mM^{-1}	45
NDI-T2 (P90)	GOx/Au	Immobilized GOx	10 nM–20 mM	0.26–16.32 NR per dec	37

PPy: polypyrrole. rGO: reduced graphene oxide. TNTA: TiO_2 nanotube array.

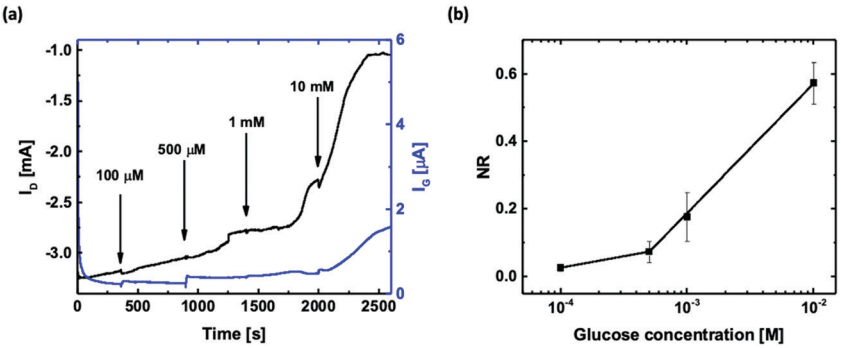

Fig. 5 (a) I_D response of a printed OECT with a GOx functionalized printed Pt gate to the addition of glucose solutions dissolved in the artificial sweat buffer. (b) Average NR of printed OECTs with the functionalized printed Pt gate to the logarithmic sweat glucose concentration. Two linear regions are observed with slopes of 0.068 NR per dec and 0.384 NR per dec for the concentration ranges of 100–500 μM and 500 μM–10 mM, respectively. The error bars represent the standard error.

Table 2 Summary of glucose biosensors for artificial or human sweat glucose analysis

Device	Sample solution	Detection range	Ref.
Printed OECT	Artificial sweat	0.1–10 mM	This work
In_2O_3 nanoribbon transistor	Artificial sweat	0.1 μM–1 mM	43
Solution gated graphene transistor	Artificial sweat	0.01–31 mM	51
Fiber electrode	Artificial sweat	0–0.5 mM	52
rGO nanocomposite electrode	Human sweat	0–2.4 mM	49
Zinc oxide (ZnO) based electrode	Human sweat	0.01–200 mg dL^{-1} (0.55 μM–11 mM)	53

the pH value of the testing solution affects the sensitivity of the glucose sensors.[47–49] As human sweat has a pH ranging from 3 to 6.5 with an average value of 4.8,[50] the pH value should be taken into consideration when developing sweat glucose sensors. Future improvement of these printed OECT based glucose sensors would include optimized channel dimensions for specific concentration ranges to improve the sensitivity and pH calibration to improve the accuracy.

Here, we have demonstrated that different OECT functionalization configurations affect the sensing range and sensitivity using the example of an OECT based glucose sensor. The choice of functionalization technique and site depends on the materials used for the device fabrication and configuration, the biorecognition element to be attached to the surface and the analyte to be detected. Physisorption may not be a suitable technique for immobilizing all types of biomolecules. For instance, chemisorption techniques are more frequently used for antibody functionalization as antibodies, which are often used in the development of immunosensors due to their high binding specificity, experience conformational changes during the adsorption process and this leads to a decrease in their bioactivity.[54] Field-effect transistors (FETs) with different functional materials benefit from various functionalization sites. An extended gate configuration is adopted by ion-sensitive field-effect transistors (ISFETs) that are based on metal-oxide semiconductor field-effect transistors (MOSFETs). In this sensor architecture, a functional extended gate can be integrated with a standard MOSFET, and gate functionalization improves their selectivity with high sensitivity.[55–57] In recent studies of SARS-CoV-2 antibody functionalized FET biosensors, carbon-based nanomaterials have been used as the active channel. Carbon based nanomaterials facilitate chemisorption with antibodies; hence, in these studies, the antibodies were directly functionalized onto the channel. These sensors were ultrasensitive to the targeted antibody–antigen binding.[58,59] Another factor to consider in biosensor design is the type of analyte solution. The stability and activity of the attached biomolecules in the analyte solution and any inhibitors or competing entities present in the analyte solution may all have an impact on the biosensor performance. Thus, based on the analyte to be detected and the type of sensor different approaches can be chosen for functionalization.

4. Conclusion

In this work, we demonstrated the use of aerosol jet printed OECTs with an in-plane Pt gate for glucose detection with four different functionalization configurations: unfunctionalized OECT with floating GOx, functionalized channel, functionalized printed Pt gate, and functionalized sputtered Pt gate. The glucose detection range and sensitivity were extracted and compared for all four functionalization configurations. The printed OECT with the printed Pt gate exhibited the best sensing performance with a large glucose detection range of 100 nM–50 mM in PBS. By using the nanoparticle-based Pt ink for gate printing and biopolymer for enzyme immobilization, the functionalized device exhibited an improved limit of

detection and a higher sensitivity to a lower glucose concentration range. The printed OECT with the functionalized printed Pt gate showed two different sensitivities of 0.022 NR per dec for 100 nM to 250 μM and 0.255 NR per dec for 250 μM to 50 mM and is the most suitable for application as a sweat glucose sensor. Glucose sensing in an artificial sweat buffer using the OECT with the functionalized printed Pt gate demonstrated a detection range of 0.1 to 10 mM, which covers the sweat glucose range, with two linear slopes of 0.068 NR per dec for 100–500 μM and 0.384 NR per dec for 500 μM–10 mM. Thus, clearly, the functionalization strategy is an extremely important parameter in designing a biosensor. For glucose detection, we found the nanostructured gate electrode functionalization to be the best option. The sensor design will have to be modified for sweat collection[60] to be used as a wearable glucose sensor. Both pH and temperature affect the GO_x enzyme activity. Thus, integrating these would improve the glucose measurement. In addition, a sensor array and/or a logic circuit may also be implemented to improve the detection accuracy. Also, it would be beneficial to be able to transfer the data from the wearable sensor to the user's cell phone and healthcare professionals. This will enable remote monitoring of patients' conditions including people in remote locations. Thus, this is an enabling technology that can be utilized for wearable sensors.

Author contributions

J. F. and M. G. conceptualized the experiments. J. F. conducted performed the biosensor fabrication and characterization. J. F. and M. G. analyzed the experimental data. A. A. F. P. conducted the AFM measurements in this study. J. F. wrote the original draft of the manuscript. J. F. and M. G. reviewed and edited the manuscript.

Conflicts of interest

We declare that there are no financial and personal conflicts related to this work.

Acknowledgements

The authors would like to acknowledge the Natural Sciences and Engineering Research Council of Canada (NSERC) for their support through the Discovery grant # 06096 to Manisha Gupta and the PGSD scholarship to Jiaxin Fan. The authors would also like to acknowledge Canadian Microelectronics Corporation (CMC microsystem) (voucher number: CMC_Microfab_6714) for providing financial support through the micro-nanotechnology (MNT) award for device fabrication and characterization.

References

1 InternationalDiabetesFederation, IDF DIABETES ATLAS, Report 9782930229874, International Diabetes Federation, 2019.
2 American Diabetes Association, *Diabetes Care*, 2019, **42**, S7–S12.
3 GrandViewResearch, *Glucose Biosensor Market Size, Share & Trends Analysis Report By End-use (Hospitals, Homecare Diagnostics, Research Institutes, Diagnostic Centers*, Clinics), By Region (U.S., UK, Germany, China, India, Brazil, Saudi Arabia, South Africa), And Segment Forecasts, 2012 - 2022, https://www.grandviewresearch.com/industry-analysis/glucose-biosensors-market, accessed May 18, 2021.
4 D. Rodbard, *Diabetes Technol. Ther.*, 2016, **18**(Suppl 2), S3–S13.
5 M. Christiansen, T. Bailey, E. Watkins, D. Liljenquist, D. Price, K. Nakamura, R. Boock and T. Peyser, *Diabetes Technol. Ther.*, 2013, **15**, 881–888.
6 B. J. Patel, B. Dave, D. Dave, P. Karmakar, M. Shah and B. Sarvaiya, *J. Int. Oral Health*, 2015, **7**, 70–76.
7 J. Moyer, D. Wilson, I. Finkelshtein, B. Wong and R. Potts, *Diabetes Technol. Ther.*, 2012, **14**, 398–402.
8 G. Scheiblin, R. Coppard, R. M. Owens, P. Mailley and G. G. Malliaras, *Adv. Mater. Technol.*, 2017, **2**, 1600141.
9 D. Majak, J. Fan and M. Gupta, *Sens. Actuators, B*, 2019, **286**, 111–118.
10 M. Ghittorelli, L. Lingstedt, P. Romele, N. I. Craciun, Z. M. Kovacs-Vajna, P. W. M. Blom and F. Torricelli, *Nat. Commun.*, 2018, **9**, 1441.
11 N. Wang, Y. Liu, Y. Fu and F. Yan, *ACS Appl. Mater. Interfaces*, 2018, **10**, 25834–25840.
12 M. Braendlein, A. M. Pappa, M. Ferro, A. Lopresti, C. Acquaviva, E. Mamessier, G. G. Malliaras and R. M. Owens, *Adv. Mater.*, 2017, **29**, 1605744.
13 S. Y. Yang, F. Cicoira, R. Byrne, F. Benito-Lopez, D. Diamond, R. M. Owens and G. G. Malliaras, *Chem. Commun.*, 2010, **46**, 7972–7974.
14 L. J. Currano, F. C. Sage, M. Hagedon, L. Hamilton, J. Patrone and K. Gerasopoulos, *Sci. Rep.*, 2018, **8**, 15890.
15 I. Gualandi, D. Tonelli, F. Mariani, E. Scavetta, M. Marzocchi and B. Fraboni, *Sci. Rep.*, 2016, **6**, 35419.
16 H. Tang, P. Lin, H. L. Chan and F. Yan, *Biosens. Bioelectron.*, 2011, **26**, 4559–4563.
17 Y. Wang, X. Qing, Q. Zhou, Y. Zhang, Q. Liu, K. Liu, W. Wang, M. Li, Z. Lu, Y. Chen and D. Wang, *Biosens. Bioelectron.*, 2017, **95**, 138–145.
18 P. Lin, X. Luo, I. M. Hsing and F. Yan, *Adv. Mater.*, 2011, **23**, 4035–4040.
19 J. Liao, S. Lin, K. Liu, Y. Yang, R. Zhang, W. Du and X. Li, *Sens. Actuators, B*, 2014, **203**, 677–682.
20 Y. Fu, N. Wang, A. Yang, H. K. Law, L. Li and F. Yan, *Adv. Mater.*, 2017, **29**, 1703787.
21 L. Bai, C. G. Elosegui, W. Li, P. Yu, J. Fei and L. Mao, *Front. Chem.*, 2019, **7**, 313.
22 N. Sandhyarani, in *Electrochemical Biosensors*, Elsevier, 2019, pp. 45–75.
23 B. D. Malhotra and M. A. Ali, in *Nanomaterials for Biosensors*, 2018, DOI: 10.1016/b978-0-323-44923-6.00001-7, pp. 1–74.
24 R. Batool, A. Rhouati, M. H. Nawaz, A. Hayat and J. L. Marty, *Biosensors*, 2019, **9**, 46.

25 N. Wang, A. Yang, Y. Fu, Y. Li and F. Yan, *Acc. Chem. Res.*, 2019, **52**, 277–287.
26 D. J. Kim, N. E. Lee, J. S. Park, I. J. Park, J. G. Kim and H. J. Cho, *Biosens. Bioelectron.*, 2010, **25**, 2477–2482.
27 R.-X. He, M. Zhang, F. Tan, P. H. M. Leung, X.-Z. Zhao, H. L. W. Chan, M. Yang and F. Yan, *J. Mater. Chem.*, 2012, **22**, 22072.
28 W. Hai, T. Goda, H. Takeuchi, S. Yamaoka, Y. Horiguchi, A. Matsumoto and Y. Miyahara, *Sens. Actuators, B*, 2018, **260**, 635–641.
29 G. Scheiblin, A. Aliane, R. Coppard, R. M. Owens, P. Mailley and G. G. Malliaras, *SPIE Organic Photonics + Electronics*, 2015, **9568**, 95681E.
30 J. Fan, C. Montemagno and M. Gupta, *Org. Electron.*, 2019, **73**, 122–129.
31 V. Bertana, G. Scordo, M. Parmeggiani, L. Scaltrito, S. Ferrero, M. G. Gomez, M. Cocuzza, D. Vurro, P. D'Angelo, S. Iannotta, C. F. Pirri and S. L. Marasso, *Sci. Rep.*, 2020, **10**, 13335.
32 D. Majak, J. Fan, S. Kang and M. Gupta, *J. Mater. Chem. B*, 2021, **9**, 2107–2117.
33 G. Tarabella, D. Vurro, S. Lai, P. D'Angelo, L. Ascari and S. Iannotta, *Flexible Printed Electron.*, 2020, **5**, 014005.
34 J. Liao, S. Lin, Y. Yang, K. Liu and W. Du, *Sens. Actuators, B*, 2015, **208**, 457–463.
35 C. Liao, M. Zhang, L. Niu, Z. Zheng and F. Yan, *J. Mater. Chem. B*, 2013, **1**, 3820–3829.
36 H. Tang, F. Yan, P. Lin, J. Xu and H. L. W. Chan, *Adv. Funct. Mater.*, 2011, **21**, 2264–2272.
37 D. Ohayon, G. Nikiforidis, A. Savva, A. Giugni, S. Wustoni, T. Palanisamy, X. Chen, I. P. Maria, E. Di Fabrizio, P. Costa, I. McCulloch and S. Inal, *Nat. Mater.*, 2020, **19**, 456–463.
38 J. T. Friedlein, M. J. Donahue, S. E. Shaheen, G. G. Malliaras and R. R. McLeod, *Adv. Mater.*, 2016, **28**, 8398–8404.
39 J. Rivnay, P. Leleux, M. Ferro, M. Sessolo, A. Williamson, D. A. Koutsouras, D. Khodagholy, M. Ramuz, X. Strakosas, R. M. Owens, C. Benar, J. M. Badier, C. Bernard and G. G. Malliaras, *Sci. Adv.*, 2015, **1**, e1400251.
40 D. A. Bernards, D. J. Macaya, M. Nikolou, J. A. DeFranco, S. Takamatsu and G. G. Malliaras, *J. Mater. Chem.*, 2008, **18**, 116–120.
41 Y. Kim, J. Do, J. Kim, S. Y. Yang, G. G. Malliaras, C. K. Ober and E. Kim, *Jpn. J. Appl. Phys.*, 2010, **49**, 01AE10.
42 M. Zhang, C. Liao, C. H. Mak, P. You, C. L. Mak and F. Yan, *Sci. Rep.*, 2015, **5**, 8311.
43 Q. Liu, Y. Liu, F. Wu, X. Cao, Z. Li, M. Alharbi, A. N. Abbas, M. R. Amer and C. Zhou, *ACS Nano*, 2018, **12**, 1170–1178.
44 A. Heller and B. Feldman, *Chem. Rev.*, 2008, **108**, 2482–2505.
45 C. Diacci, J. W. Lee, P. Janson, G. Dufil, G. Méhes, M. Berggren, D. T. Simon and E. Stavrinidou, *Adv. Mater. Technol.*, 2019, **5**, 1900262.
46 S. K. Kanakamedala, H. T. Alshakhouri, M. Agarwal and M. A. DeCoster, *Sens. Actuators, B*, 2011, **157**, 92–97.
47 A. Bhide, S. Muthukumar and S. Prasad, *Biosens. Bioelectron.*, 2018, **117**, 537–545.
48 H. Lee, C. Song, Y. S. Hong, M. S. Kim, H. R. Cho, T. Kang, K. Shin, S. H. Choi, T. Hyeon and D. H. Kim, *Sci. Adv.*, 2017, **3**, e1601314.
49 X. Xuan, H. S. Yoon and J. Y. Park, *Biosens. Bioelectron.*, 2018, **109**, 75–82.
50 J. L. Matousek and K. L. Campbell, *Vet. Dermatol.*, 2002, **13**, 293–300.
51 M. Ma, Y. Zhou, J. Li, Z. Ge, H. He, T. Tao, Z. Cai, X. Wang, G. Chang and Y. He, *Analyst*, 2020, **145**, 887–896.
52 Y. Zhao, Q. Zhai, D. Dong, T. An, S. Gong, Q. Shi and W. Cheng, *Anal. Chem.*, 2019, **91**, 6569–6576.
53 R. D. Munje, S. Muthukumar and S. Prasad, *Sens. Actuators, B*, 2017, **238**, 482–490.
54 S. K. Vashist and J. H. Luong, in *Handbook of Immunoassay Technologies*, Elsevier, 2018, pp. 19–46.
55 J. Kwon, B.-H. Lee, S.-Y. Kim, J.-Y. Park, H. Bae, Y.-K. Choi and J.-H. Ahn, *ACS Sens.*, 2019, **4**, 1724–1729.
56 T. Minamiki, T. Minami, R. Kurita, O. Niwa, S. I. Wakida, K. Fukuda, D. Kumaki and S. Tokito, *Materials*, 2014, **7**, 6843–6852.
57 S. Sheibani, L. Capua, S. Kamaei, S. S. A. Akbari, J. Zhang, H. Guerin and A. M. Ionescu, *Communications Materials*, 2021, **2**, 1–10.
58 G. Seo, G. Lee, M. J. Kim, S. H. Baek, M. Choi, K. B. Ku, C. S. Lee, S. Jun, D. Park, H. G. Kim, S. J. Kim, J. O. Lee, B. T. Kim, E. C. Park and S. I. Kim, *ACS Nano*, 2020, **14**, 5135–5142.
59 W. Shao, M. R. Shurin, S. E. Wheeler, X. He and A. Star, *ACS Appl. Mater. Interfaces*, 2021, **13**, 10321–10327.
60 P. Makaram, D. Owens and J. Aceros, *Diagnostics*, 2014, **4**, 27–46.